



HAL
open science

Superconducting Gravimeter Observations Show That a Satellite-Derived Snow Depth Image Improves the Simulation of the Snow Water Equivalent Evolution in a High Alpine Site

F Koch, S Gascoin, K Achmüller, P Schattan, C Deschamps-berger, M Lehning, T Rehm, K Schulz, C Voigt

► **To cite this version:**

F Koch, S Gascoin, K Achmüller, P Schattan, C Deschamps-berger, et al.. Superconducting Gravimeter Observations Show That a Satellite-Derived Snow Depth Image Improves the Simulation of the Snow Water Equivalent Evolution in a High Alpine Site. *Geophysical Research Letters*, 2024, 51, 10.1029/2024gl112483. hal-04860916

HAL Id: hal-04860916

<https://hal.science/hal-04860916v1>

Submitted on 1 Jan 2025

HAL is a multi-disciplinary open access archive for the deposit and dissemination of scientific research documents, whether they are published or not. The documents may come from teaching and research institutions in France or abroad, or from public or private research centers.

L'archive ouverte pluridisciplinaire **HAL**, est destinée au dépôt et à la diffusion de documents scientifiques de niveau recherche, publiés ou non, émanant des établissements d'enseignement et de recherche français ou étrangers, des laboratoires publics ou privés.



Distributed under a Creative Commons Attribution - NonCommercial - NoDerivatives 4.0 International License

Geophysical Research Letters[®]



RESEARCH LETTER

10.1029/2024GL112483

F. Koch and S. Gascoïn contributed equally.

Key Points:

- Evaluation of a distributed physically based snow model using superconducting gravimetry in a high alpine area
- Precipitation scaling based on a single satellite snow depth image significantly improves the simulated gravity signal of the snowpack
- Accurate spatial distribution of snow depth is found to be key to simulate snow mass (SWE) evolution in complex alpine terrain

Supporting Information:

Supporting Information may be found in the online version of this article.

Correspondence to:

F. Koch and S. Gascoïn,
franziska.koch@boku.ac.at;
simon.gascoin@univ-tlse3.fr

Citation:

Koch, F., Gascoïn, S., Achmüller, K., Schattan, P., Wetzel, K.-F., Deschamps-Berger, C., et al. (2024). Superconducting gravimeter observations show that a satellite-derived snow depth image improves the simulation of the snow water equivalent evolution in a high alpine site. *Geophysical Research Letters*, 51, e2024GL112483. <https://doi.org/10.1029/2024GL112483>

Received 10 SEP 2024

Accepted 23 OCT 2024

Author Contributions:

Conceptualization: F. Koch, S. Gascoïn

Data curation: F. Koch, S. Gascoïn, K. Achmüller, C. Voigt









Funding acquisition: F. Koch, S. Gascoïn, K. Schulz, C. Voigt

Methodology: F. Koch, S. Gascoïn, C. Voigt

© 2024. The Author(s).

This is an open access article under the terms of the [Creative Commons Attribution-NonCommercial-NoDerivs License](#), which permits use and distribution in any medium, provided the original work is properly cited, the use is non-commercial and no modifications or adaptations are made.

Superconducting Gravimeter Observations Show That a Satellite-Derived Snow Depth Image Improves the Simulation of the Snow Water Equivalent Evolution in a High Alpine Site

F. Koch¹ , S. Gascoïn² , K. Achmüller^{3,4}, P. Schattan¹, K.-F. Wetzel⁵ , C. Deschamps-Berger⁶ , M. Lehning⁷ , T. Rehm⁸ , K. Schulz¹ , and C. Voigt³ 

¹Institute of Hydrology and Water Management, University of Natural Resources and Life Sciences (BOKU), Vienna, Austria, ²CESBIO, Université de Toulouse, CNRS/CNES/IRD/INRA/UPS, Toulouse Cedex, France, ³GFZ German Research Centre for Geosciences, Section 1.2 Global Geomonitoring and Gravity Field, Potsdam, Germany, ⁴Institute of Geodesy and Geoinformation Science, Technische Universität Berlin, Berlin, Germany, ⁵Institute of Geography, Augsburg University, Augsburg, Germany, ⁶Pyrenean Institute of Ecology, Zaragoza, Spain, ⁷WSL Institute for Snow and Avalanche Research SLF, Davos Dorf, Switzerland, ⁸Environmental Research Station Schneefernerhaus (UFS), Zugspitze, Germany

Abstract The lack of accurate information on the spatiotemporal variations of snow water equivalent (SWE) in mountain catchments remains a key problem in snow hydrology and water resources management. This is partly because there is no sensor to measure SWE beyond local scale. At Mt. Zugspitze, Germany, a superconducting gravimeter senses the gravity effect of the seasonal snow, reflecting the temporal evolution of SWE in a few kilometers scale radius. We used this new observation to evaluate two configurations of the Alpine3D distributed snow model. In the default run, the model was forced with meteorological station data. In the second run, we applied precipitation correction based on an 8 m resolution snow depth image derived from satellite observations (Pléiades). The snow depth image strongly improved the simulation of the snowpack gravity effect during the melt season. This result suggests that satellite observations can enhance SWE analyses in mountains with limited infrastructure.

Plain Language Summary This study addresses the challenge of accurately computing the amount of water stored in snow (known as snow water equivalent or SWE) in mountainous areas, which is important for managing water resources. Typically, there are no tools that can measure SWE across large areas in complex high alpine surroundings, only at specific points. However, at Mt. Zugspitze at the border of Germany and Austria, a special device called a superconducting gravimeter can detect changes in gravity caused by the snow, providing a way to estimate SWE over large areas. We used data from this gravimeter to test two versions of a snow model called Alpine3D. In the first version, the model relied only on weather station data. In the second version, we improved the model by using satellite images to adjust the amount and spatial distribution of precipitation (snowfall) in the model. The results showed that the model gets more accurate by using satellite data to predict SWE changes during the melting season. This finding suggests that satellite images could be a useful tool for analyzing SWE in mountainous regions with limited infrastructure.

1. Introduction

Estimating the spatial distribution of snow water equivalent (SWE) in mountain catchments is often presented as the holy grail of snow hydrologists (Dozier et al., 2016). This is because the spatial distribution of SWE controls the magnitude and timing of snowmelt runoff (Freudiger et al., 2017). Recent progresses in climate modeling, remote sensing and data assimilation have enabled significant progress toward this endeavor (Gascoïn et al., 2024). High resolution studies used snow depth images from airborne or satellite sensors to evaluate their simulations since there is no operational method to measure SWE distribution in complex terrain (Berg et al., 2024; Haddjeri et al., 2024; Hedrick et al., 2018; Margulis et al., 2019; Quéno et al., 2023; Sourp et al., 2024). Using snow depth as a proxy to evaluate snow hydrology models assumes that the snowpack density is accurately simulated by the model, although the spread in snow density between different models can be significant (Raleigh & Small, 2017). In addition, snow depth images are infrequent for several reasons including weather conditions, the cost of airborne campaigns or the narrow swath of very-high resolution satellites (Eberhard et al., 2021).

Software: F. Koch, S. Gascoin, K. Achmüller, P. Schattan, K.-F. Wetzel, C. Deschamps-Berger, M. Lehning, C. Voigt
Validation: F. Koch, K. Achmüller, T. Rehm, C. Voigt
Visualization: F. Koch, S. Gascoin, K. Achmüller, P. Schattan
Writing – original draft: F. Koch, S. Gascoin
Writing – review & editing: F. Koch, S. Gascoin, K. Achmüller, P. Schattan, K.-F. Wetzel, C. Deschamps-Berger, M. Lehning, T. Rehm, K. Schulz, C. Voigt

Monitoring the evolution of SWE with in-situ techniques is challenging as measurements are only available at very few locations, mainly due to costs and difficult accessibility. In case no SWE measurements are available, the measurement of point-scale snow depth, if available, together with numerical modeling of the density evolution, is among the most reliable local SWE estimation methods (Egli et al., 2009). In addition, novel measuring techniques using Global Navigation Satellite System (GNSS) or Cosmic Ray Neutron Sensing (CNRS) can overcome some of the issues of conventional sensors, in particular regarding costs, maintenance and, regarding CNRS, also the measurement footprint, but can still cover only single locations within a greater area of interest like a hydrological catchment (Koch et al., 2019; Schattan et al., 2019).

For the direct and non-invasive monitoring of integral water storage variations for areas up to a few kilometers scale radius around the observation site, superconducting gravimeters (Chaffaut et al., 2022; Güntner et al., 2017; Kumar et al., 2023) and spring gravimeters (Jacob et al., 2010; Pivetta et al., 2024) have been used, for example, for studying the water balance, storage-discharge relationships, and karst hydrosystems. Spring gravimeters are transportable and less expensive than superconducting gravimeters, but they lack long-term stability due to irregular drift behavior. Voigt et al. (2021) introduced in this regard a superconducting gravimeter at the high-alpine Zugspitze Geodynamic Observatory Germany (ZUGOG) in the European Alps. This can be seen as a novel sensor for snow hydrology since the snowpack is the primary contributor to seasonal gravimetric signal changes. It enables to sense SWE continuously as an integral of a larger, kilometer-scale contribution area in complex high-alpine terrain.

In this study, we explicitly compared measurements of the superconducting gravimeter installed at ZUGOG to evaluate two different physically based snowpack simulation schemes. The comparison of the simulations with the gravimetric measurements shows that assimilating a snow depth image derived from satellite photogrammetry in the snowpack model improves the contribution of snow mass variations throughout the melt season. This underlines that the spatial distribution of snow depth at fine scale (8 m) is a key driver of the spatially integrated SWE evolution during the melt season.

2. Data and Methods

2.1. Study Area Zugspitze

The study was carried out in the Zugspitze massif at the border of Germany and Austria in the European Northern Calcareous Alps. The selected high alpine area of 20.8 km² around Mt. Zugspitze (2.962 m a.s.l.) is characterized by complex topography and steep slopes (Figures 1a and 1b). Most of the upper part of the site is covered by no or rather sparse alpine vegetation above approx. 2,000 m a.s.l. Below and down to the lowest point of the site (1.430 m a.s.l.), dwarf mountain pine and scarce coniferous tree stands are predominant. Hydrologically, the site is characterized by a long snow season and karstic discharge conditions through bedded limestone layers (Lauber & Goldscheider, 2014; Wetzel, 2004). Three small glaciers are situated within the study site: the Northern Schneeferner and the Southern Schneeferner (no more glacier status since 2022) as well as the Höllentalferner, which covered a total area of 0.35 km² in 2018 (Mayer et al., 2021). Permafrost is present in the steep north-facing rock walls of Mt. Zugspitze (Krautblatter et al., 2010). The site has an excellent scientific infrastructure provided by the Environmental Research Station Schneefernerhaus (UFS) situated directly within the site including a dense network of hydro-meteorological stations. Taking advantage of these unique settings, various snow and hydrological studies were carried out (e.g., Ferrarin et al., 2023; Härer et al., 2018; Hürkamp et al., 2019; Weber et al., 2021).

2.2. Gravimetric Signal

In December 2018, a superconducting gravimeter was installed in the Zugspitze Geodynamic Observatory Germany (ZUGOG) at the summit of Mt. Zugspitze. Its location on the highest peak in the region is optimal to study cryospheric and hydrological processes as all land water mass variations occur below the gravimeter. For the derivation of the cryo-hydrological signal, the raw observation data in 1 s time resolution were processed according to Voigt et al. (2021). This includes the conversion from voltage to gravity variations with an amplitude factor and a linear drift estimation based on absolute gravimeter measurements (Timmen et al., 2021) as well as the reduction of solid Earth and ocean tides and non-tidal gravity effects from atmospheric mass redistributions and Earth rotation. The precision of this observation method is known to be better than 1 nm s⁻² (10⁻⁹ m s⁻²) in the time domain. The gravity residuals result from the cryospheric and hydrological mass variations over a

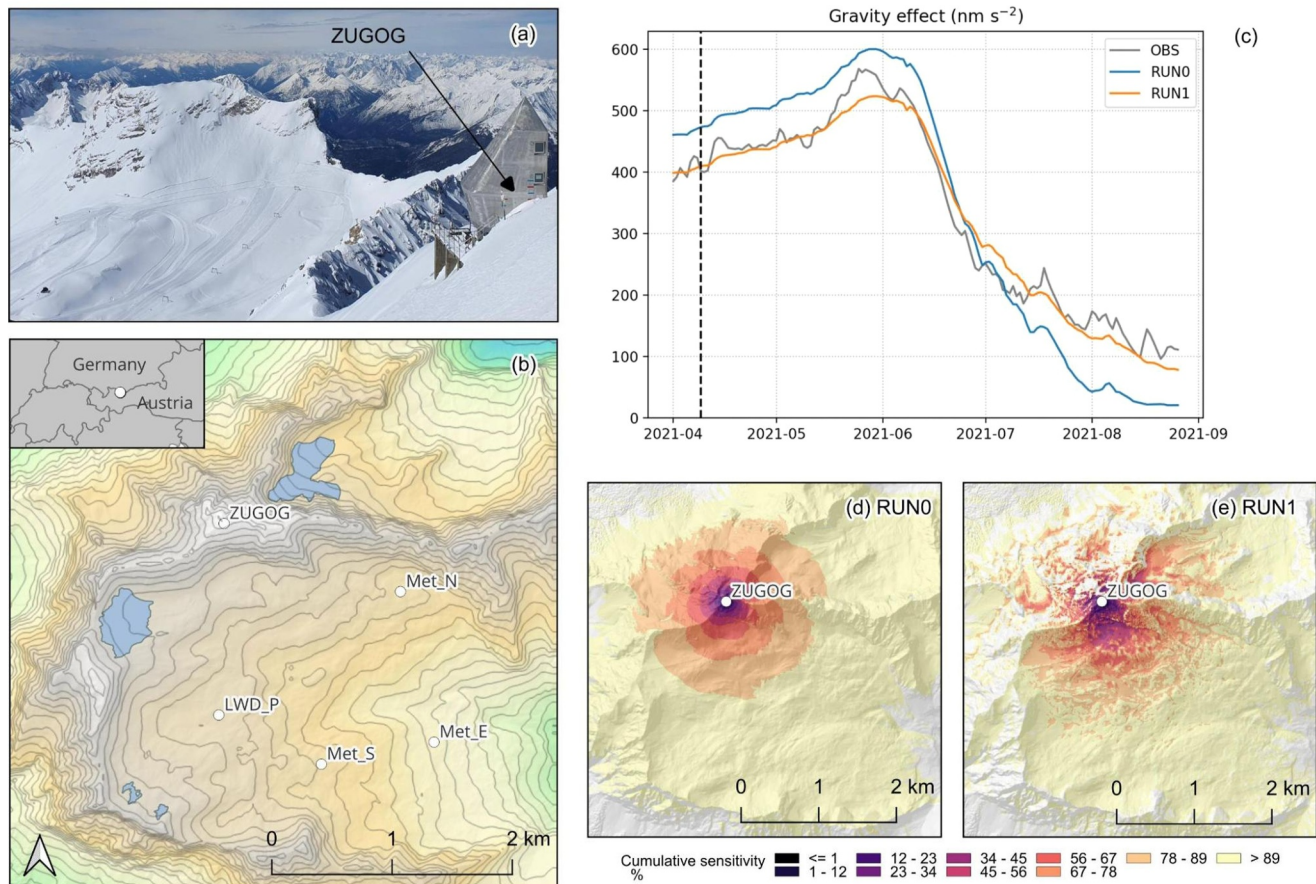


Figure 1. (a) Photograph showing the building of the Zugspitze Geodetic Observatory Germany (ZUGOG) on top of Mt. Zugspitze and the snow-covered upper part of the Zugspitzplatt (26 Apr 2024). (b) Topographic overview of the Zugspitze study site including the locations of the ZUGOG, the meteorological stations LWD_P, Met_N, Met_S and Met_E and the glaciated areas (glacier extent of 2018). (c) Observed cryo-hydro gravity residuals derived with the superconducting gravimeter at the ZUGOG (OBS), integral snow-gravity effect calculated from the Alpine3D simulations RUN0 and RUN1 for the contributing areas at each time step. (d) and (e) Cumulative snow-gravimetric sensitivity calculated from Alpine3D RUN0 (d) and RUN1 (e) showing the contributing area as the cumulative snow-gravimetric sensitivity in % on 1 June 2021, weighted with the maximum of the gravity signal that occurred on 25 May 2021 (=100%), cf. Section 2.5.

spatiotemporally varying contributing area. The data are available since 29 December 2018 at a temporal resolution of 1 hr. For this study, we used the dataset from 1 September 2020–1 September 2021.

According to Newton's law of gravitation, the gravity effect is most sensitive to mass variations close to the instrument with a signal attenuation of $1/r^2$ (r being the distance between gravimeter and source mass). In addition, the gravimeter is only sensitive to vertical acceleration changes, which further reduce the contribution of distant areas (Creutzfeldt et al., 2008; Van Camp et al., 2017). Overall, the snowpack is the primary contributor to the gravimetric signal at the Zugspitze site. The spatial extent (i.e., footprint) of snow cover changes to the gravimeter measurements is not fixed as it depends on the snow mass change itself. As soon as the site is more or less snow-free, also in the upper parts of the site close to the gravimeter, other hydrological storages and fluxes like precipitation events cascading through the karst system as well as karst water body retention can be observed predominantly in the gravimetric signal. On a long-term scale of several years, ice mass losses can be detected showing an overall negative long-term reduction of the cryo-hydro gravity residuals.

2.3. Snow Depth Image

We generated an image of the snow depth (height of snow, HS) at 8 m resolution over the study area by differencing a snow-on and a snow-off digital elevation model (see Figure S1 in Supporting Information S1). We computed the snow-on DEM from a stereoscopic pair of panchromatic Pléiades images acquired on 9 April 2021 using the same software and configuration that were successfully evaluated in a previous study (Beyer et al., 2019;

Deschamps-Berger et al., 2020). We extracted the snow-off DEM from an airborne lidar DEM acquired in summer 2020 provided by the federal state of Tyrol (Austria). Then, we aligned the snow-on DEM on the snow-off DEM by finding the translation vector, which minimized the normalized median absolute deviation on snow-free, glacier-free, lake-free and forest-free areas using the Nelder-Mead algorithm (Virtanen et al., 2020). For the determination of the snow-free areas, we used a supervised classification, that is, by training a statistical model on 26 polygonal samples labeled with the following classes: snow, no-snow, shaded snow, shaded no-snow as done by Shaw et al. (2020). We collected these samples manually by visual inspection. To perform this task, we used a color composite of the green, red and near-infrared bands from the Pléiades multispectral image as it allows a better discrimination of surface properties despite its lower resolution (2 m) than the panchromatic image (0.5 m). The classifier used all the spectral bands of the multispectral image (blue, green, red and near-infrared). We orthorectified beforehand the multispectral image on the Pléiades DEM to ensure an accurate coregistration of both images (DEM and land cover). We determined the tree covered areas by extracting pixels with a strictly positive value in the Tree Cover Density product from Copernicus Land Monitoring Service (European Environment Agency, 2020). The glacier areas were obtained from the Bavarian glacier inventory of 2018 (Mayer et al., 2021). We mapped the Eibsee lake area in the North of the site manually.

We set HS to zero where the land cover classification indicated no-snow after resampling it to 8 m using the mode value from the contributing 2 m pixels. As we noticed that the HS image presented abnormal values where the Pléiades panchromatic images were saturated, we set to no-data the HS values where the value of the back panchromatic image from the stereo pair was greater than 4,080 (i.e., close the maximum, 4,096). We used the back image of the stereopair as it is more prone to sun exposure due to its viewing geometry. Furthermore, we applied the same translation to the saturation mask as we did for the DEM to align saturated pixels with abnormal snow depth values. We also set to no-data every HS value, which exceeded three standard deviations of the HS distribution (9.5 m). Finally, we interpolated no-data values using an inverse distance weighting interpolation algorithm with a radius of 10 pixels (GDAL/OGR contributors, 2024).

2.4. Snowpack Simulations

We applied the spatially distributed physically based snow model Alpine3D (Lehning et al., 2006) with its core, the one dimensional multilayer model SNOWPACK (Bartelt & Lehning, 2002), to simulate SWE and HS in the entire study domain at a 8 m spatial and a 1 hr temporal resolution. Alpine3D was successfully used for various applications, including snowpack modeling at different scales and complexities (Schlögl et al., 2016; Wever et al., 2015), snow-hydrological modeling (Bavay et al., 2013; Pulka et al., 2024) and ski resort management (Ebner et al., 2021).

As meteorological input, we used hourly data of air temperature, precipitation, relative humidity, wind speed and direction and incoming shortwave radiation from five automatic weather stations (AWS) within and in close vicinity of the study site Zugspitze (see further information of meteorological stations in Table S1 in Supporting Information S1) for the time period 1 September 2020–1 September 2021. MeteIO was used to spatially interpolate the meteorological input data (Bavay & Egger, 2014). The algorithms applied for the calculation and spatial interpolation of these data are listed in Table S2 in Supporting Information S1. Regarding the spatial model input datasets we used the same airborne lidar digital elevation model as in Section 2.3, and the CORINE Land Cover dataset of 2018 (European Environment Agency, 2019). Both datasets were rescaled to the 8 m spatial resolution of the modeling domain (20.8 km²). This high spatial resolution was computationally still well feasible for the multilayer hourly snowpack simulations.

Alpine3D was run with two different configurations hereafter referred to as RUN0 and RUN1. RUN0 used the default configuration of Alpine3D as introduced above. RUN1 used in addition a solid precipitation scaling algorithm based on a single snow depth map (Vögeli et al., 2016) to describe the spatial distribution of snow depth more realistically. This approach uses spatially distributed correction factors for each time step to the solid precipitation field based on the patterns of the Pléiades snow depth image from 9 April 2021. We applied the precipitation scaling for solid precipitation at each raster cell with information of satellite-based HS including a quantitative precipitation correction based on the average HS difference of the simulation and the snow depth image (Richter et al., 2021). In addition, a correction factor between the observed and simulated HS per raster cell was applied. For raster cells with no satellite-based HS information, for example, at the lower parts of the study site with tree stands, the default Alpine3D scheme was applied, however, taking mass and energy conservation

over the entire study domain into account. Overall, the solid precipitation scaling approach aims to improve the accuracy of the spatial distribution of the simulated HS and SWE, mimicking the preferential deposition of snow due to wind and gravitational transport at the date of the snow depth image (Lehning et al., 2008). As snow patterns remain quite stable over time, especially during the melt season, this approach can be used for the entire melt season if the HS image was taken close to peak SWE (Brauchli et al., 2017).

Station-based validation of the simulated HS and SWE was carried out on a daily basis at five snow measurement sites within the study site (Table S3 in Supporting Information S1) providing in total five HS recordings and one SWE measurement.

2.5. Simulated Snow-Gravimetric Signal

The gravity effect of snow at ZUGOG was calculated for every raster cell for RUN0 and RUN1 by using topography information from the DEM and the simulated SWE (i.e., the snow mass on top of each raster cell), and Newton's law of gravitation (as formulated in Nagy et al., 2000) considering the signal attenuation with distance and direction to the gravimeter. Summing up the contribution of each raster cell in the study area gives the integral snow-gravity effect. The cumulative snow-gravimetric sensitivity was calculated as follows: the gravimetric contributions of each raster cell were added in descending order of their absolute value until the difference between this sum and the total gravity effect is less than 1 nm s^{-2} (truncation criterion according to Voigt et al., 2021). Once the gravimetric contribution of a raster cell has been added to the sum, this raster cell receives the current sum of the snow-gravity effect as an entry, weighted with the maximum of the gravity signal that occurred on 25 May 2021 (=100%) to obtain percentage values.

As superconducting gravimetry is a relative technique, it measures only the temporal variations of the gravity field. Therefore, we centered the signal measured by the gravimeter to the mean value of both simulated time series over the study period for each RUN:

$$S_c(t) = S(t) - \bar{S}_z + \frac{\bar{S}_0 + \bar{S}_1}{2}$$

where $S(t)$ is the original value of the simulated gravimetric signal from RUN0 (or RUN1) per time step, \bar{S}_z is the mean value of the gravimetric time series from Section 2.2, \bar{S}_0 and \bar{S}_1 the mean values of the simulated gravimetric signal from RUN0 and RUN1, and $S_c(t)$ is the centered gravimetric signal per time step (nm s^{-2}) that we used to evaluate the simulations. We set the comparison period between the Alpine3D runs and the gravimetric observation from 1 April 2021–26 August 2021, which encompasses the Pléiades acquisition close to its beginning (9 April 2021), accumulation peak and the melt season, which is the focus of our study. We selected 26 August as the end date since early snowfalls were observed in the area from 27 August 2021.

3. Results

Comparing the simulated snow-gravity effect of RUN0 and RUN1, the results show that RUN1, using satellite-derived precipitation scaling based on a snow depth image, simulated better the signal measured by the superconducting gravimeter than RUN0, the default Alpine3D simulation (Figure 1c). In particular, the decrease of the observed gravity residuals during the melt season is better captured (i.e., after peak SWE occurring near 1 June 2021), whereas the accumulation shows a similar evolution for both runs. The better performance of RUN1 is also underlined by the RMSE between the observed cryo-hydro gravity residuals and the simulated snow gravimetric effect for RUN0 with 5.1 nm s^{-2} and for RUN1 with 1.8 nm s^{-2} , calculated for the centered gravimetric signals. This is due to the fact that the assimilation of the HS image changed the spatial patterns of the simulated SWE and consequently also the simulated cumulative snow-gravimetric sensitivity in RUN1. The gravimetric contribution of RUN0, however, is rather homogeneous and dominated by the distance from the gravimeter accounting to the decline in elevation, whereas RUN1 exhibits larger spatial heterogeneity as shown in Figures 1d and 1e. In addition, Figure S2 in Supporting Information S1 compares the simulated snow cover patterns with those captured by Sentinel-2 for three dates during the melting season. The snow covered areas simulated with RUN1 follow very well the pattern of the satellite observation, whereas RUN0 shows a distinctly different behavior regarding snow covered areas and melt out.

For both runs, the contributing area and the integral snow gravity effect changes over time during the melting season (Figure S3 in Supporting Information S1). The radius describing the maximum extent of the contributing area around the gravimeter is, however, quite constant with more than approximately 3.25 km in slant direction, exemplarily for 1 April, 1 May and 1 June 2021 for both runs. Only toward the end of the melting season on 1 July, this maximum radius shows a decrease with less than 3 km in RUN1 and even less than 2.5 km in RUN0 (Figure S4 in Supporting Information S1). Compared to the maximum extent, the area from which 95% of the signal originates is already considerably smaller being in the range of approximately 2 km for both RUN0 and RUN1 as the gravity effect of the snow mass is declining with squared distance. This is even more obvious in close vicinity, as for example, the area from which 50% of the signal originates is in the range of 300 m for RUN0 and 500 m for RUN1, respectively. RUN0 has a shorter melting period compared to RUN1, which is underlined by a faster decline of the simulated integral snow-gravity effect shown in Figure 1c. Regarding RUN1, the satellite-based precipitation scaling reproduced the observed spatial distribution and maxima in snow accumulation, which prolonged the melt season, being in line with the gravimetric signal.

Figure 2 shows that RUN1 also outperformed RUN0 in terms of HS and SWE at the in situ stations. The improvement in RUN1 is especially evident after the date of the Pléiades acquisition. At all stations, we found also that the satellite-derived snow depths compare well with the in situ observations. HS fits for both runs well at the stations LWD_P and Met_N and SWE is captured well at the LWD_P station for both runs, however, reaches a better maximum SWE for RUN1. However, RUN0 is off for the entire winter season for the stations Met_E, Met_S and ZUGOG. These three stations have in common that the topography in their surroundings is more complex than for the other two stations. RUN0 results in more snow than simulated with the satellite-derived snow depth distribution pattern in RUN1 at these locations. However, although RUN1 fits well in the melting phase, it shows a slight delay of a couple of days in complete melt out at the stations, which is also confirmed in Figure S2 in Supporting Information S1 in comparison with satellite snow covered area.

Figure 3 illustrates at four specific dates (1 April, 1 May, 1 June, and 1 July 2021), how the assimilation of the Pléiades HS reshaped the spatial distribution of SWE by increasing its variance with elevation in RUN1 with respect to RUN0 and how it impacted its evolution. RUN0 shows, in general, low SWE variance, however, with a slight increase per altitude and over all four time steps, and a higher median SWE for higher altitudes compared to RUN1. RUN1 has its highest spread and median SWE over these dates in the altitude range of 2.400–2.600 m a.s.l. Corresponding to the upper Zugspitzplatt with less steep slopes than above, but still high topographic variability in terrain. Overall, the steeper parts of the site including mountain peaks and crests are situated above 2.600 m a.s.l., where the SWE median in RUN1 is reduced, compared to areas between 2.200 and 2.600 m a.s.l. In lower parts of the site, the median and variance declines due to earlier melt out in the presented time steps.

4. Discussion and Conclusion

The observation of a superconducting gravimeter installed at Mt. Zugspitze provided a fully independent validation method to compare cryo-hydro gravity residuals, as a snow mass proxy during the snow-covered period, with physically based SWE simulations converted into snow gravimetric sensitivities for contribution areas at a few kilometers radius scale around the gravimeter. This is a novel possibility to evaluate SWE in high-alpine, complex terrain.

The results suggest that assimilating Pléiades snow depth caused a redistribution of the snow mass in the study area, which led to a better simulation of the gravity changes around the gravimeter within the contributing area. In particular, the higher spatial heterogeneity of SWE in RUN1 induced a different SWE evolution, which better matched the declining gravimetric signal of the snowpack after peak SWE. This finding confirms previous knowledge about the key influence of snow depth spatial distribution on the evolution of the catchment-scale SWE during the melt season (Brauchli et al., 2017; Freudiger et al., 2017). The default model RUN0 generated SWE patterns that were strongly correlated with elevation, reflecting the elevation-based lapse rate parameterizations of meteorological forcing in MeteolO. Previous studies have shown that a low spatial heterogeneity in SWE results in overestimated melt rate in mountain catchments (Clark et al., 2011), but the gravimetric observations provide another fully independent observational argument to support this concept. Consequently, the assimilation of Pléiades snow depth data into Alpine 3D also improves the understanding of the spatial contributions of the gravimetric signal.

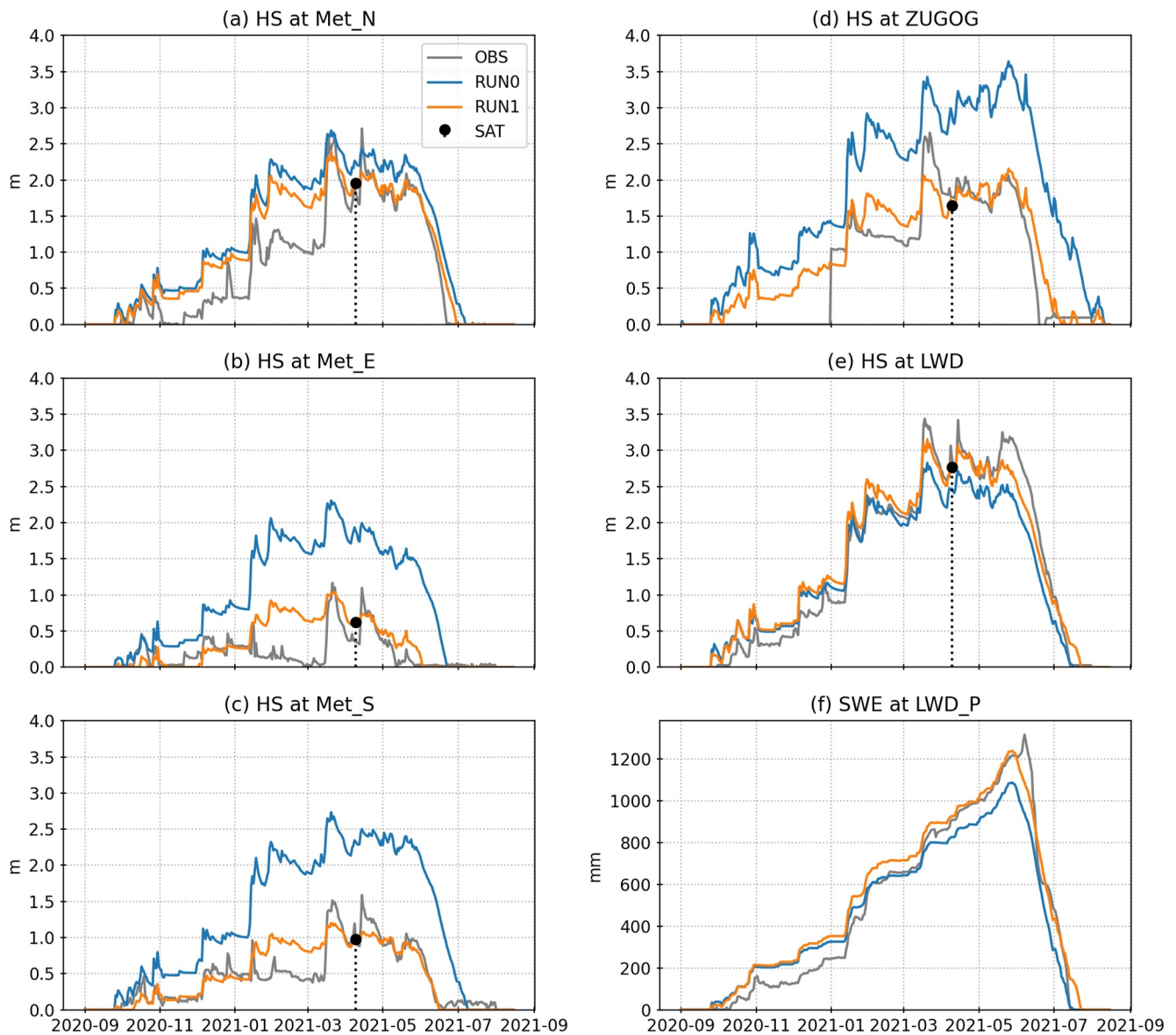


Figure 2. (a)–(e) Comparison of snow depth (HS) observed at station (OBS), derived from satellite (SAT) and simulated with the Alpine3D RUN0 and RUN1 at the station (a) Met_N, (b) Met_E, (c) Met_S, (d) ZUGOG, (e) LWD_P. (f) Comparison of snow water equivalent (SWE) observed at station and simulated with the Alpine3D RUN0 and RUN1 at LWD_P.

As the study site was largely covered by snow during spring, and also during summer in the upper part (Figure S2 in Supporting Information S1) being very sensitive to the gravimeter due to $1/r^2$, the gravity residuals represent predominantly the changes of the snow storage during the study period, whereas other potential fluxes and storages are neglected here. However, the curve of the gravity observations shows more fluctuations indicating potential effects other than the simulated snow-gravimetric effect of RUN0 and RUN1 (Figure 1c). As reported by Voigt et al. (2021), the measurements can be influenced by local effects in the direct vicinity of the instrument, which are not captured by the simulations. This can be additional snow accumulating in front of ZUGOG due to eventual clearance from a nearby visitors' platform with a snow blower or wind effects on snow around the building. In contrast to this snow-dominated season 2020/21, in seasons with less or no snow lasting until summer close to the gravimeter, other cryo-hydrological changes, which can also be located further away, can be more prevalent in the gravity signal, being subject of future research.

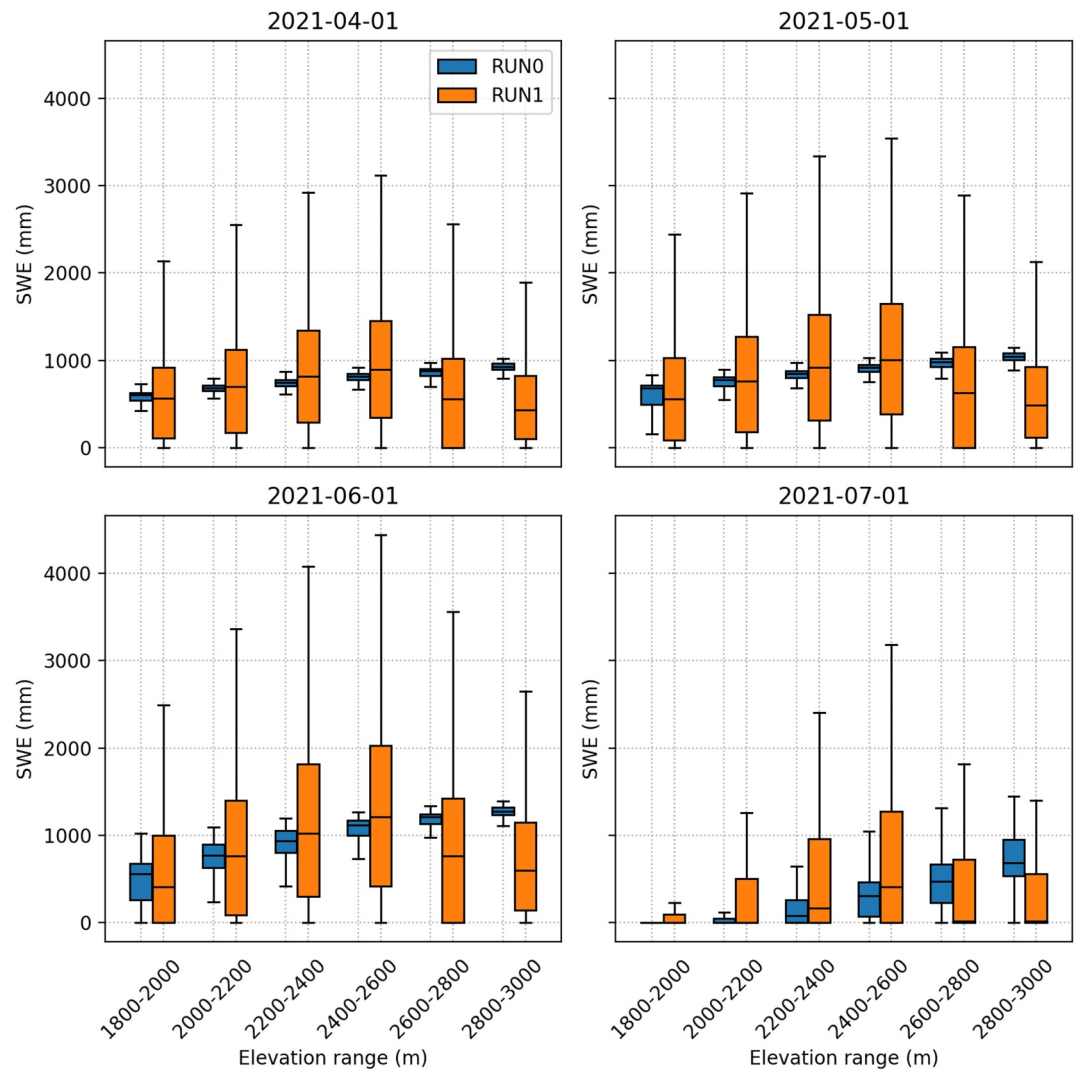


Figure 3. Distribution of the snow water equivalent (SWE) simulated with the Alpine3D RUN0 and RUN1 over different elevation ranges (in m a.s.l.) for 1 April, 1 May, 1 June, and 1 July 2021. The box extends from the first quartile to the third quartile of the data, with a line at the median. The whiskers extend from the box to the farthest data point lying within 1.5x the interquartile range from the box.

The assimilation method that we used to correct the snow patterns and SWE is numerically efficient and therefore allows the simulation of the snowpack at high resolution, but it suffers from several limitations. First, it does not take into account the uncertainty of the assimilated snow depth, although it can exceed 1 m in steep terrain (Deschamps-Berger et al., 2020). Regarding Figure S2 in Supporting Information S1, the agreement between satellite snow covered areas and RUN1 is good. However, in mid-August, it seems that the model slightly overestimates the snow, which could be caused by a too high HS estimation of the snow depth image taken on 9 April 2021 at some deeper snow patches or changing physical properties of the snow, for example, reduced albedo caused by Sahara dust or other impurities during the late melt-out season. As it is a deterministic approach, it does not provide information on the model output uncertainties unlike more advanced assimilation methods (Alonso-González et al., 2022). Another issue is that our approach corrects only precipitation to fit the snow depth at the pixel level, which assumes that all other processes are accurately simulated including uncertain processes like wind transport, preferential deposition and gravitational transport (Vögeli et al., 2016). We cannot exclude that this correction did not compensate for other model errors and that we got “the right answer for the wrong reason” due to the multiple possibilities of equifinality when assimilating snow depth with a process-based model like Alpine3D.

In this study, the Alpine3D runs were forced with automatic weather station data. However, progress in climate modeling and the availability of climate reanalysis with increasing accuracy should allow similar applications in mountains without in-situ meteorological measurements or airborne campaigns (Sourp et al., 2024; Weber et al., 2021), which are subject to future comparisons and potential transferability for snow simulations in ungauged catchments. The results for the melting period in 2021, demonstrate that the combination of Alpine3D with a Pléiades-derived snow depth spring image (RUN1) enables obtaining an accurate representation of the snowpack evolution. This paves the way to high resolution spatially distributed snow simulations in data-scarce regions.

The availability of superconducting gravimeter measurements provide valuable observations for comparing different SWE simulations and assimilation schemes. It gives the snow-hydrology community for the first time the possibility to evaluate snow mass over a few kilometers scale in complex, high-alpine terrain. Moreover, the gravimetric signal as an integral observation can also give valuable insights for precipitation quantification and correction of precipitation products in high-alpine areas, where many products suffer from severe precipitation deficits. The present assimilation approach offers a tool to disentangle the areas contributing to the integrated snow-gravimetric signal enabling the assignment of the regions and snow processes represented in the signal. Overall, this study shows that observations based on a superconducting gravimeter open new avenues in mountain hydrology to better model snow processes. In addition, considering superconducting gravimeter signals for the evaluation of hydrological modelling enables to investigate and capture other water storage changes and fluxes like sublimation/evaporation, single rain events and the total precipitation, ice melt, karst water retention or rainfall-runoff process in more detail in such high alpine environments tackling the major challenge of separating the individual hydrological signals.

Data Availability Statement

The data to reproduce all (Figures 1–3 and Figures S1 to S4 in Supporting Information S1) is available at Zenodo (Koch et al., 2024).

The airborne lidar-based digital elevation model (DEM) data are available from <https://www.tirol.gv.at/sicherheit/geoinformation/geodaten-tiris/laserscandaten/>. Copernicus Data (tree cover density and land cover) are taken from (European Environment Agency, 2020). The glacier outlines are available from <http://www.bayerische-gletscher.de/>.

The models Alpine3D, SNOWPACK and MeteIO are available under the LPGL version three open source license: <https://code.wsl.ch/snow-models>.

The Ames StereoPipeline-2.6.2 is available from Beyer et al. (2019).

Raw gravity and atmospheric pressure data from the OSG 052 at ZUGOG have been published (Voigt et al., 2019) and are available from the International Geodynamics and Earth Tide Service database hosted by the Information System and Data Center at GFZ (Voigt et al., 2016). For the processing of the gravimetric data the following airborne lidar-based digital elevation model (DEM) data were used: <https://www.tirol.gv.at/sicherheit/geoinformation/geodaten-tiris/laserscandaten/> (Austria and close vicinity of ZUGOG) and <https://geodaten.bayern.de/opengeodata/OpenDataDetail.html?pn=dgml> (Germany).

The meteorological model input from the German Weather Service (Deutscher Wetterdienst, DWD) are available at: https://www.dwd.de/DE/klimaumwelt/cdc/cdc_node.html; the LWD data are available on request at the Bavarian Avalanche Service (<https://lawinenwarndienst.bayern.de/>); the meteorological model input from Geosphere Austria are available at: <https://data.hub.geosphere.at/group/stationsdaten>.

References

- Alonso-González, E., Aalstad, K., Baba, M. W., Revuelto, J., López-Moreno, J. I., Fiddes, J., et al. (2022). The multiple snow data assimilation system (MuSA v1.0). *Geoscientific Model Development*, 15(24), 9127–9155. <https://doi.org/10.5194/gmd-15-9127-2022>
- Bartelt, P., & Lehning, M. (2002). A physical SNOWPACK model for the Swiss avalanche warning: Part I: Numerical model. *Cold Regions Science and Technology*, 35(3), 123–145. [https://doi.org/10.1016/S0165-232X\(02\)00074-5](https://doi.org/10.1016/S0165-232X(02)00074-5)
- Bavay, M., & Egger, T. (2014). MeteIO 2.4.2: A preprocessing library for meteorological data. *Geoscientific Model Development*, 7(6), 3135–3151. <https://doi.org/10.5194/gmd-7-3135-2014>
- Bavay, M., Grünewald, T., & Lehning, M. (2013). Response of snow cover and runoff to climate change in high Alpine catchments of Eastern Switzerland. *Advances in Water Resources*, 55, 4–16. <https://doi.org/10.1016/j.advwatres.2012.12.009>

Acknowledgments

This research was funded by the Austrian Science Fund (FWF) [Grant 10.55776/I6489, FWF-DFG Weave project G-MONARCH, project start in 2023]. For open access purposes, the authors have applied a CC BY public copyright license to any author accepted manuscript version arising from this submission. We are grateful for the funding received under the French-Austrian Campus France Amadeus/OeAD WTZ project FRAU SNOW (FR 07/2023) allowing travels for the authors F. Koch and S. Gascoin to Toulouse, France and Vienna, Austria for joint research stays. In addition, we are grateful for the granting of the Bourse du gouvernement français in 2021, allowing travels for the author F. Koch to Toulouse, France, which was the kickoff of the collaboration between the two first authors F. Koch and S. Gascoin. We thank the staff of the Environmental Research Station Schneefernerhaus (UFS), Deutsche Funkturm, Bayerische Zugspitzbahn and Tiroler Zugspitzbahn, for their personnel and technical support. We gratefully obtained meteorological and snow station data from the Bavarian Avalanche Service (LWD) and the UFS. Pléiades images were acquired thanks to DINAMIS (Dispositif Institutionnel National d'Approvisionnement Mutualisé en Imagerie Satellitaire). S. Gascoin also acknowledges support from CNES/TOSCA. We thank Carla Braitenberg and Juan Ignacio López Moreno for their constructive and valuable reviews that helped to significantly improve the manuscript.

- Berg, J., Reynolds, D., Quéno, L., Jonas, T., Lehning, M., & Mott, R. (2024). A seasonal snowpack model forced with dynamically downscaled forcing data resolves hydrologically relevant accumulation patterns. *Frontiers in Earth Science*, *12*, 1393260. <https://doi.org/10.3389/feart.2024.1393260>
- Beyer, R., Alexandrov, O., & McMichael, S. (2019). *NeoGeographyToolkit/StereoPipeline: Asp 2.6.2*. Version v2.6.2. Zenodo. <https://doi.org/10.5281/zenodo.3247734>
- Brauchli, T., Trujillo, E., Huwald, H., & Lehning, M. (2017). Influence of slope-scale snowmelt on catchment response simulated with the Alpine3D model. *Water Resources Research*, *53*(12), 10723–10739. <https://doi.org/10.1002/2017WR021278>
- Chaffaut, Q., Hinderer, J., Masson, F., Viville, D., Pasquet, S., Boy, J. P., et al. (2022). New insights on water storage dynamics in a mountainous catchment from superconducting gravimetry. *Geophysical Journal International*, *228*(1), 432–446. <https://doi.org/10.1093/gji/ggab328>
- Clark, M. P., Hendrikx, J., Slater, A. G., Kavetski, D., Anderson, B., Cullen, N. J., et al. (2011). Representing spatial variability of snow water equivalent in hydrologic and land-surface models: A review. *Water Resources Research*, *47*(7). <https://doi.org/10.1029/2011WR010745>
- Creutzfeldt, B., Güntner, A., Klügel, T., & Wziontek, H. (2008). Simulating the influence of water storage changes on the superconducting gravimeter of the Geodetic Observatory Wettzell, Germany. *Geophysics*, *73*(6), WA95–WA104. <https://doi.org/10.1190/1.2992508>
- Deschamps-Berger, C., Gascoïn, S., Berthier, E., Deems, J., Gutmann, E., Dehecq, A., et al. (2020). Snow depth mapping from stereo satellite imagery in mountainous terrain: Evaluation using airborne Laser-scanning data. *The Cryosphere*, *14*(9), 2925–2940. <https://doi.org/10.5194/tc-14-2925-2020>
- Dozier, J., Bair, E. H., & Davis, R. E. (2016). Estimating the spatial distribution of snow water equivalent in the world's mountains. *WIREs Water*, *3*(3), 461–474. <https://doi.org/10.1002/wat2.1140>
- Eberhard, L. A., Sirguey, P., Miller, A., Marty, M., Schindler, K., Stoffel, A., & Bühler, Y. (2021). Intercomparison of photogrammetric platforms for spatially continuous snow depth mapping. *The Cryosphere*, *15*(1), 69–94. <https://doi.org/10.5194/tc-15-69-2021>
- Ebner, P. P., Koch, F., Premier, V., Marin, C., Hanzer, F., Carmagnola, C. M., et al. (2021). Evaluating a prediction system for snow management. *The Cryosphere*, *15*(8), 3949–3973. <https://doi.org/10.5194/tc-15-3949-2021>
- Egli, L., Jonas, T., & Meister, R. (2009). Comparison of different automatic methods for estimating snow water equivalent. *Cold Regions Science and Technology*, *57*(2), 107–115. <https://doi.org/10.1016/j.coldregions.2009.02.008>
- European Environment Agency. (2019). *CORINE land cover 2018 (raster 100 m), europe, 6-yearly - version 2020_20ul, May 2020 (version 20.01) [GeoTIFF]*. European Environment Agency. <https://doi.org/10.2909/960998C1-1870-4E82-8051-6485205EBBAC>
- European Environment Agency. (2020). (Version 02.00) [GeoTIFF]. European Environment Agency. <https://doi.org/10.2909/48677DA-D605-423E-93A9-680760AB6791>. *Tree cover density 2018 (raster 10 m), europe, 3-yearly, sep. 2020*
- Ferrarin, L., Schulz, K., Bocchiola, D., & Koch, F. (2023). Morphological indexes to describe snow-cover patterns in a high-alpine area. *Annals of Glaciology*, 1–12. <https://doi.org/10.1017/aog.2023.62>
- Freudiger, D., Kohn, I., Seibert, J., Stahl, K., & Weiler, M. (2017). Snow redistribution for the hydrological modeling of alpine catchments: Snow redistribution for hydrological modeling. *Wiley Interdisciplinary Reviews: Water*, *4*(5), e1232. <https://doi.org/10.1002/wat2.1232>
- Gascoïn, S., Luoju, K., Nagler, T., Lievens, H., Masiokas, M., Jonas, T., et al. (2024). Remote sensing of mountain snow from space: Status and recommendations. *Frontiers in Earth Science*, *12*. <https://doi.org/10.3389/feart.2024.1381323>
- GDAL/OGR contributors. (2024). GDAL/OGR geospatial data abstraction software library. *Open Source Geospatial Foundation*. <https://doi.org/10.5281/zenodo.5884351>
- Güntner, A., Reich, M., Mikolaj, M., Creutzfeldt, B., Schroeder, S., & Wziontek, H. (2017). Landscape-scale water balance monitoring with an iGrav superconducting gravimeter in a field enclosure. *Hydrology and Earth System Sciences*, *21*(6), 3167–3182. <https://doi.org/10.5194/hess-21-3167-2017>
- Haddjeri, A., Baron, M., Lafaysse, M., Le Toumelin, L., Deschamps-Berger, C., Vionnet, V., et al. (2024). Analyzing the sensitivity of a blowing snow model (SnowPappus) to precipitation forcing, blowing snow, and spatial resolution. *The Cryosphere*, *18*(7), 3081–3116. <https://doi.org/10.5194/tc-18-3081-2024>
- Härer, S., Bernhardt, M., Siebers, M., & Schulz, K. (2018). On the need for a time- and location-dependent estimation of the NDSI threshold value for reducing existing uncertainties in snow cover maps at different scales. *The Cryosphere*, *12*(5), 1629–1642. <https://doi.org/10.5194/tc-12-1629-2018>
- Hedrick, A. R., Marks, D., Havens, S., Robertson, M., Johnson, M., Sandusky, M., et al. (2018). Direct insertion of NASA airborne snow observatory-derived snow depth time series into the iSnobal energy balance snow model. *Water Resources Research*, *54*(10), 8045–8063. <https://doi.org/10.1029/2018WR023190>
- Hürkamp, K., Zentner, N., Reckerth, A., Weishaupt, S., Wetzel, K.-F., Tschiersch, J., & Stumpp, C. (2019). Spatial and temporal variability of snow isotopic composition on Mt. Zugspitze, bavarian alps, Germany. *Journal of Hydrology and Hydromechanics*, *67*(1), 49–58. <https://doi.org/10.2478/johh-2018-0019>
- Jacob, T., Bayer, R., Chery, J., & Le Moigne, N. (2010). Time-lapse microgravity surveys reveal water storage heterogeneity of a karst aquifer. *Journal of Geophysical Research*, *115*(B6). <https://doi.org/10.1029/2009JB006616>
- Koch, F., Gascoïn, S., Achmüller, K., Schattan, P., & Voigt, C. (2024). Dataset for the publication “Superconducting gravimeter observations show that satellite-derived snow depth image improves the simulation of the snow water equivalent evolution in a high alpine site” (Version v1) [Dataset]. <https://doi.org/10.5281/zenodo.13475075>
- Koch, F., Henkel, P., Appel, F., Schmid, L., Bach, H., Lamm, M., et al. (2019). Retrieval of snow water equivalent, liquid water content, and snow height of dry and wet snow by combining GPS signal attenuation and time delay. *Water Resources Research*, *55*(5), 4465–4487. <https://doi.org/10.1029/2018WR024431>
- Krautblatter, M., Verleysdonk, S., Flores-Orozco, A., & Kemna, A. (2010). Temperature-calibrated imaging of seasonal changes in permafrost rock walls by quantitative electrical resistivity tomography (Zugspitze, German/Austrian Alps). *Journal of Geophysical Research*, *115*(F2). <https://doi.org/10.1029/2008JF001209>
- Kumar, S., Rosat, S., Hinderer, J., Mouyen, M., Boy, J.-P., & Israil, M. (2023). Delineation of aquifer boundary by two vertical superconducting gravimeters in a karst hydrosystem, France. *Pure and Applied Geophysics*, *180*(2), 611–628. <https://doi.org/10.1007/s00024-022-03186-7>
- Lauber, U., & Goldscheider, N. (2014). Use of artificial and natural tracers to assess groundwater transit-time distribution and flow systems in a high-alpine karst system (Wetterstein Mountains, Germany). *Hydrogeology Journal*, *22*(8), 1807–1824. <https://doi.org/10.1007/s10040-014-1173-6>
- Lehning, M., Löwe, H., Ryser, M., & Raderschall, N. (2008). Inhomogeneous precipitation distribution and snow transport in steep terrain. *Water Resources Research*, *44*(7). <https://doi.org/10.1029/2007WR006545>
- Lehning, M., Völksch, I., Gustafsson, D., Nguyen, T. A., Stähli, M., & Zappa, M. (2006). ALPINE3D: A detailed model of mountain surface processes and its application to snow hydrology. *Hydrological Processes*, *20*(10), 2111–2128. <https://doi.org/10.1002/hyp.6204>

- Margulis, S. A., Fang, Y., Li, D., Lettenmaier, D. P., & Andreadis, K. (2019). The utility of infrequent snow depth images for deriving continuous space-time estimates of seasonal snow water equivalent. *Geophysical Research Letters*, *46*(10), 5331–5340. <https://doi.org/10.1029/2019GL082507>
- Mayer, C., Weber, M., Wendt, A., & Hagg, W. (2021). Die bayerischen Gletscher, die verbliebenen Eisreserven Deutschlands. *Polarforschung*, *89*(1), 1–7. <https://doi.org/10.5194/polif-89-1-2021>
- Nagy, D., Papp, G., & Benedek, J. (2000). The gravitational potential and its derivatives for the prism. *Journal of Geodesy*, *74*(7–8), 552–560. <https://doi.org/10.1007/s001900000116>
- Pivetta, T., Braitenberg, C., Gabrovšek, F., Gabriel, G., & Meurers, B. (2024). Gravimetry and hydrologic data to constrain the hydrodynamics of a karstic area: The Škocjan Caves study case. *Journal of Hydrology*, *629*, 130453. <https://doi.org/10.1016/j.jhydrol.2023.130453>
- Pulka, T., Herrmegger, M., Ehrendorfer, C., Lücking, S., Avanzi, F., Formayer, H., et al. (2024). Evaluating precipitation corrections to enhance high-alpine hydrological modeling for hydropower. <https://doi.org/10.2139/ssrn.4823086>
- Quéno, L., Mott, R., Morin, P., Cluzet, B., Mazzotti, G., & Jonas, T. (2023). Snow redistribution in an intermediate-complexity snow hydrology modelling framework. *EGUsphere*, 1–32. <https://doi.org/10.5194/egusphere-2023-2071>
- Raleigh, M. S., & Small, E. E. (2017). Snowpack density modeling is the primary source of uncertainty when mapping basin-wide SWE with lidar. *Geophysical Research Letters*, *44*(8), 3700–3709. <https://doi.org/10.1002/2016GL071999>
- Richter, B., Schweizer, J., Rotach, M. W., & van Herwijnen, A. (2021). Modeling spatially distributed snow instability at a regional scale using Alpine3D. *Journal of Glaciology*, *67*(266), 1147–1162. <https://doi.org/10.1017/jog.2021.61>
- Schattan, P., Köhli, M., Schrön, M., Baroni, G., & Oswald, S. E. (2019). Sensing area-average snow water equivalent with cosmic-ray neutrons: The influence of fractional snow cover. *Water Resources Research*, *55*(12), 10796–10812. <https://doi.org/10.1029/2019WR025647>
- Schlögl, S., Marty, C., Bavay, M., & Lehning, M. (2016). Sensitivity of Alpine3D modeled snow cover to modifications in DEM resolution, station coverage and meteorological input quantities. *Environmental Modelling and Software*, *83*(Supplement C), 387–396. <https://doi.org/10.1016/j.envsoft.2016.02.017>
- Shaw, T. E., Gascoïn, S., Mendoza, P. A., Pellicciotti, F., & McPhee, J. (2020). Snow depth patterns in a high mountain andean catchment from satellite optical tristereoscopic remote sensing. *Water Resources Research*, *56*(2), e2019WR024880. <https://doi.org/10.1029/2019WR024880>
- Sourp, L., Gascoïn, S., Jarlan, L., Pedinotti, V., Bormann, K. J., & Baba, M. W. (2024). Evaluation of high resolution snowpack simulations from global datasets and comparison with Sentinel-1 snow depth retrievals in the Sierra Nevada (pp. 1–22). *EGUsphere*. <https://doi.org/10.5194/egusphere-2024-791>
- Timmen, L., Gerlach, C., Rehm, T., Völksen, C., & Voigt, C. (2021). Geodetic-gravimetric monitoring of mountain uplift and hydrological variations at Zugspitze and wank mountains (bavarian alps, Germany). *Remote Sensing*, *13*(5), 918. <https://doi.org/10.3390/rs13050918>
- Van Camp, M., de Viron, O., Watlet, A., Meurers, B., Francis, O., & Caudron, C. (2017). Geophysics from terrestrial time-variable gravity measurements. *Reviews of Geophysics*, *55*(4), 938–992. <https://doi.org/10.1002/2017RG000566>
- Virtanen, P., Gommers, R., Oliphant, T. E., Haberland, M., Reddy, T., Cournapeau, D., et al. (2020). SciPy 1.0: Fundamental algorithms for scientific computing in Python. *Nature Methods*, *17*(3), 261–272. <https://doi.org/10.1038/s41592-019-0686-2>
- Vögeli, C., Lehning, M., Wever, N., & Bavay, M. (2016). Scaling precipitation input to spatially distributed hydrological models by measured snow distribution. *Frontiers in Earth Science*, *4*. <https://doi.org/10.3389/feart.2016.00108>
- Voigt, C., Förste, C., Wziontek, H., Crossley, D., Meurers, B., Pálincás, V., et al. (2016). Report on the data base of the international Geodynamics and Earth tide Service (IGETS). Scientific Technical Report STR - Data; 16/08. *Deutsches GeoForschungszentrum GFZ*. <https://doi.org/10.2312/GFZ.B103-16087>
- Voigt, C., Pflug, H., Förste, C., Flechtner, F., & Rehm, T. (2019). Superconducting gravimeter data from Zugspitze - level 1 (version 001) [Application/octet-stream,application/octet-stream]. *GFZ Data Services*. <https://doi.org/10.5880/IGETS.ZU.L1.001>
- Voigt, C., Schulz, K., Koch, F., Wetzel, K.-F., Timmen, L., Rehm, T., et al. (2021). Technical note: Introduction of a superconducting gravimeter as novel hydrological sensor for the Alpine research catchment Zugspitze. *Hydrology and Earth System Sciences*, *25*(9), 5047–5064. <https://doi.org/10.5194/hess-25-5047-2021>
- Weber, M., Koch, F., Bernhardt, M., & Schulz, K. (2021). The evaluation of the potential of global data products for snow hydrological modelling in ungauged high-alpine catchments. *Hydrology and Earth System Sciences*, *25*(5), 2869–2894. <https://doi.org/10.5194/hess-25-2869-2021>
- Wetzel, K.-F. (2004). On the Hydrology of the Partnach Area in the Wetterstein Mountains (Bavarian Alps) (Zur Hydrologie des Partnach-Ursprungs im Wettersteingebirge). *Erdkunde*, *58*(2), 172–186. <https://doi.org/10.3112/erdkunde.2004.02.05>
- Wever, N., Schmid, L., Heilig, A., Eisen, O., Fierz, C., & Lehning, M. (2015). Verification of the multi-layer SNOWPACK model with different water transport schemes. *The Cryosphere*, *9*(6), 2271–2293. <https://doi.org/10.5194/tc-9-2271-2015>

References From the Supporting Information

- Dilley, A. C., & O'Brien, D. M. (1998). Estimating downward clear sky long-wave irradiance at the surface from screen temperature and precipitable water. *Quarterly Journal of the Royal Meteorological Society*, *124*(549), 1391–1401. <https://doi.org/10.1002/qj.49712454903>
- Goodison, B. E., Louie, P. Y., & Yang, D. (1998). WMO solid precipitation measurement intercomparison. Retrieved from <https://globalcryospherewatch.org/bestpractices/docs/WMOtd872.pdf>
- Unsworth, M. H., & Monteith, J. L. (1975). Long-wave radiation at the ground I. Angular distribution of incoming radiation. *Quarterly Journal of the Royal Meteorological Society*, *101*(427), 13–24. <https://doi.org/10.1002/qj.49710142703>